PTEP

Prog. Theor. Exp. Phys. **2023** 053B01(14 pages)
DOI: 10.1093/ptep/ptad036

IYBSSD2022
International Year
of Basic Sciences
for Sustainable Development

Observability of triple top quark signal at future hadron colliders

Ijaz Ahmed[1], Nazima Bi[2], M. W. Ather[3], and M. S. Amjad[3]

[1] *Applied Physics Department, Federal Urdu University of Arts, Science and Technology, Islamabad 44000, Pakistan*
[2] *Physics Department, Riphah International University, Sector I-14, Hajj Complex, Islamabad 44000, Pakistan*
[3] *NUTECH School of Applied Sciences and Humanities, National University of Technology, Sector I-12, Islamabad 44000, Pakistan*
* E-mail: ijaz.ahmed@fuuast.edu.pk

Received March 10, 2023; Revised March 3, 2023; Accepted March 10, 2023; Published March 11, 2023

The Standard Model (SM) cross-sections for the production of single top quarks, top-quark pairs, triple top quarks, and four top quarks at three different center-of-mass energies, i.e. $\sqrt{s} = 7$, 10, and 14 TeV, at existing particle colliders as well as at future hadron colliders, are studied. A fully kinematic analysis with the optimized preselection cuts along with invariant mass reconstruction of top quarks is performed for triple-top production processes $pp \to ttt W$, $tttd$, and $tttb$ in the presence of the SM background. All three signal processes are forced to decay in fully hadronic mode. The studies are performed for the High-Luminosity Large Hadron Collider (HL−LHC) at $\sqrt{s} = 14$ TeV and for the High-Energy LHC (HE−LHC) at $\sqrt{s} = 27$ TeV. The signal to background ratio and signal significance of all signal and background processes are estimated for both the scenarios. It is found that the chances of signal observability at the HE−LHC are higher than those at the HL−LHC.
PACS numbers: 12.60.Fr, 14.80.Fd

Subject Index B57

1. Introduction

Top-quark characteristics are one of the most important aspects of the Standard Model (SM). It is also possible that top quarks will play a key role in breaking electroweak symmetry, which is responsible for the masses of all fundamental particles. Top quarks have some unique properties including enormously large mass, and they could be a gateway to the discovery of new physics. Also, owing to their extremely short lifetime, their bare quark properties can be studied as they decay before hadronization. Top quarks have been observed to be produced singly through weak interactions and in top pairs through strong interactions [1,2]. Due to their large mass, high collision energy is necessary to produce top quarks. At the Large Hadron Collider (LHC), a large number of top quarks were produced at energies of 7 TeV and 8 TeV. As a result, top characteristics have been investigated in great detail and precision. These findings are consistent with the SM's predictions for top quarks. However, in the Beyond the Standard

Funded by SCOAP[3]. SCOAP[3] and OUP support the goals of the International Year of Basic Sciences for Sustainable Development.

Model (BSM) regime, there has been a limited focus on the triple top particularly. For example, [3] discusses the triple top in view of searches for scalar bosons. The authors propose that the triple top may be studied in the signature of three leptons plus three b-jets, as confirmation. They also argue that a triple-top search at the High-Luminosity LHC (HL-LHC) could conditionally cover the full mass range up to 700 GeV. Also [4] includes a discussion on the triple top in the context of flavor-changing neutral current (FCNC) induced by the Z‘-boson. The Z‘-boson produced in association with a single top quark and decaying to a $t\bar{t}$ could decay to a triple-top final state. This might become dominant as compared to a single top under certain coupling conditions. However, there's also the possibility that it remains negligible under different coupling conditions.

Since its discovery [5] in Fermilab at the Tevatron collider by the CDF and D0 Collaborations [6–8], the top quark has remained the heaviest elementary particle. It completed the third-generation structure of the SM and opened the top quark physics area [9]. The large mass of the top quark makes phenomenology so important as it is usually the most closely related to new physics proposals in the BSM regime [10]. In addition, it has a very short lifetime and decays without hadronization [11], making top quark physics a unique playground to study a bare quark [12]. At the Tevatron collider and LHC, many properties of the top quark were studied, including the production mechanism and basic properties such as mass, width, and decay [13].

For both Fermilab's Tevatron and CERN's LHC, top-pair and single-top production have been extensively studied. Single-top production is also of interest, especially for the SM V_{tb} mixing element, and was observed at the Tevatron [14,15]. Several search programs involve the top quark, which is commonly considered sensitive to new physics on the TeV scale, e.g. top-quark pair production of the opposite sign or same sign, single top-quark production, and four top-quark production. Unfortunately, triple top-quark production still does not receive much attention. Of all the current top-quark-related physics search programs, the triple-top production is very special [16]. We measure single-top, top-pair, triple-top, and four-top quark cross-sections at different mass energy centers in this paper and address the discovery potential of triple-top events at the LHC and how new physics can significantly affect this channel.

2. Single top-quark production

In Beyond the Standard Model (BSM), single top-quark production is also susceptible to physics including charged Wtb vertex structure, new gauge bosons, new heavy quarks, and top-quark neutral currents that change flavor [17,18]. There are three different single top-quark production modes at the LHC which are t-channel, s-channel, and tW-channel production [19,21] whose cross sections are shown in Fig. 1. Lowest-order Feynman diagrams for single top-quark production through weak interaction are shown in Fig. 2. In Table 1, the cross section due to single top production are listed.

3. Top-pair production

The production of triple top quarks uses a mixture of single top quarks and pairs [15]. According to the SM, the strong interactions generate top pairs at the Tevatron, as well as at the LHC [14], and single top-quark production is generated mostly through electroweak interaction with the W-boson [19,20]. Top-quark pairs are formed by quark–antiquark ($q\bar{q} \rightarrow t\bar{t}$) annihilation and gluon–gluon fusion ($gg \rightarrow t\bar{t}$). In the Tevatron collider, the first is the most dominant, whereas in the LHC, the second is dominant [9,19,22]. Figure 3 shows the Feyn-

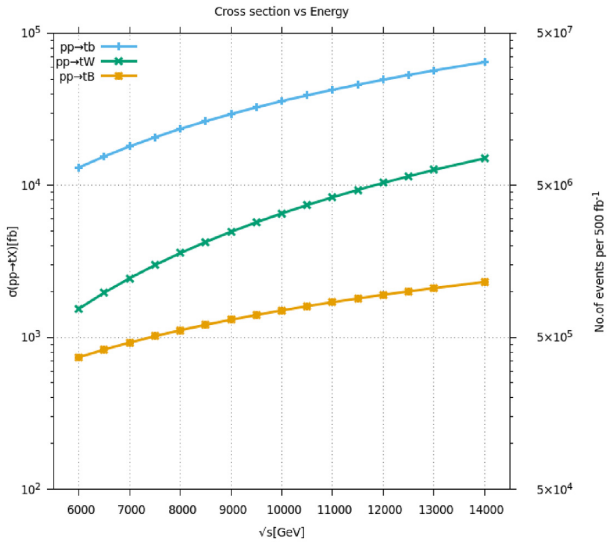

Fig. 1. Cross-section for single-top production in the SM for different LHC center-of-mass energies.

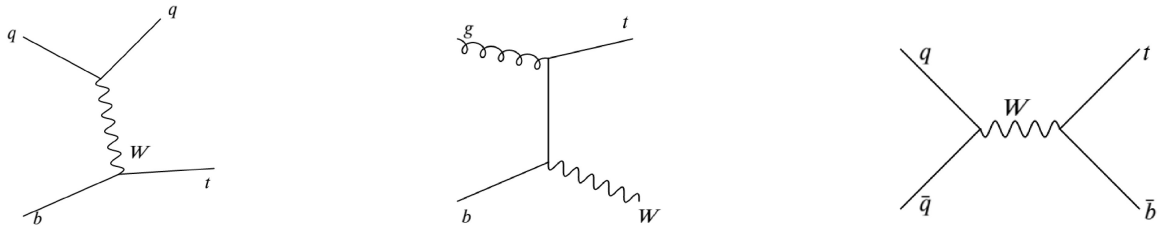

Fig. 2. Feynman diagram of single top-quark production in the SM: t-channel (left), W-associated production or tW-channel (center), and s-channel (right).

Table 1. Cross-section for single top-quark production through weak interaction at the LHC.

Process	No. of diagrams	$\sqrt{s} = 7$ TeV	$\sqrt{s} = 10$ TeV	$\sqrt{s} = 14$ TeV
$\sigma(t$-channel)[fb]	4	1.8039×10^4	3.5832×10^4	4.9552×10^4
$\sigma(s$-channel)[fb]	4	9.2312×10^2	1.5027×10^3	2.3140×10^3
$\sigma(tW$-channel)[fb]	4	2.9856×10^3	6.5386×10^3	1.5074×10^4

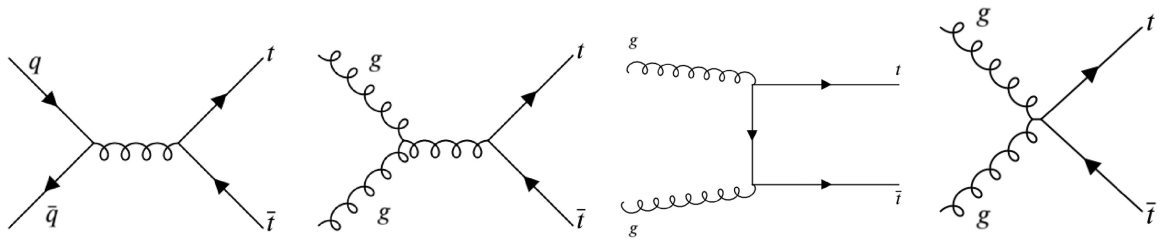

Fig. 3. Lowest-order Feynman diagrams contributing to top-quark pair production at the LHC.

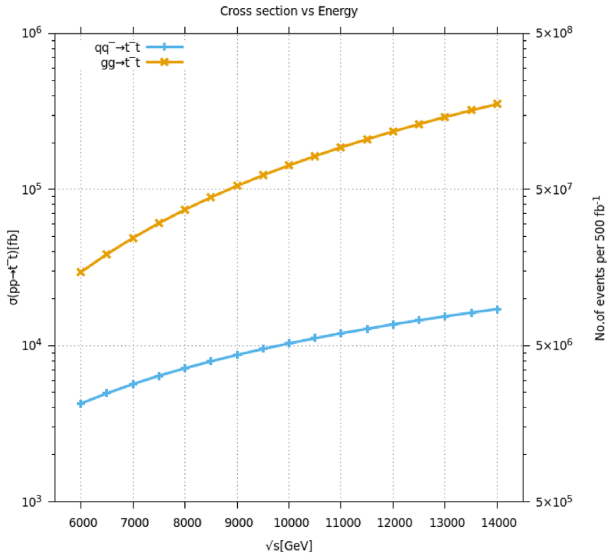

Fig. 4. Top-quark pair production cross-section for quark–antiquark annihilation and gluon–gluon fusion processes at the LHC.

Table 2. Cross-section for top-quark pair production through strong interaction at the LHC.

Process	No. of Feynman diagrams	$\sqrt{s}$ =7 TeV	$\sqrt{s}$ = 10 TeV	$\sqrt{s}$ = 14 TeV
$\sigma(q\bar{q} \to t\bar{t})$[fb]	38	5.6691×10^3	1.0336×10^4	1.7143×10^4
$\sigma(gg \to t\bar{t})$[fb]	3	4.8952×10^4	1.4287×10^5	3.5331×10^5

Table 3. Cross-section for triple top-quark production at the LHC.

Process	No. of diagrams	$\sqrt{s}$ = 7 TeV	$\sqrt{s}$ = 10 TeV	$\sqrt{s}$ = 14 TeV
$\sigma(pp \to t\bar{t} + W^-)$[fb]	118	1.8039×10^4	3.5832×10^4	4.9552×10^4
$\sigma(pp \to t\bar{t} + d)$[fb]	76	9.2312×10^2	1.5027×10^3	2.3140×10^3
$\sigma(pp \to t\bar{t} + \bar{b})$[fb]	36	2.9856×10^3	6.5386×10^3	1.5074×10^4

man diagram of the lowest order for top-pair production by strong interaction and Fig. 4 shows its corresponding cross section.

We can see from Table 2 that the production of top-quark pairs in the LHC is much greater than that of Tevatron because of higher collision energy and higher luminosity [22].

4. Triple top-quark production

The triple top quark has three different production modes in the SM at the LHC [23]. The three production modes of the triple top quark are $pp \to 3t + W^{\pm}$, $pp \to 3t + \bar{b}$, and $pp \to 3t + d$ [15]. Table 3 shows that the triple top-quark cross-section is low. Due to its small cross-section, triple top-quark production is very rare [24]. In Fig. 5 and Fig. 6 the Feynman diagrams and cross section are shown for triple top quark production.

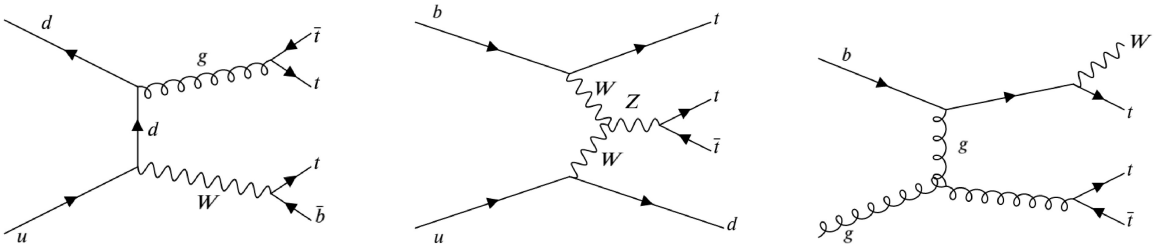

Fig. 5. Feynman diagrams for triple top-quark production in the SM at the LHC corresponding to three processes.

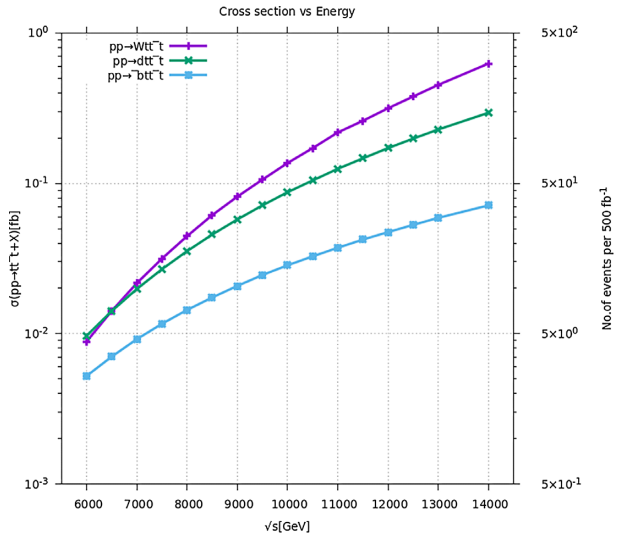

Fig. 6. Cross-section for triple-top production in the SM for different LHC center-of-mass energies.

Table 4. Cross-section for four top-quark production at the LHC.

Process	No. of diagrams	$\sqrt{s} = 7$ TeV	$\sqrt{s} = 10$ TeV	$\sqrt{s} = 14$ TeV
$\sigma(q\bar{q} \to t\bar{t}t\bar{t})$[fb]	54	5.6691×10^3	$1.0336E \times 10^4$	1.7143×10^4
$\sigma(gg \to t\bar{t}t\bar{t})$[fb]	54	4.8952×10^4	1.4287×10^5	3.5331×10^5

The triple-top cross-section is very small compared to the SM prediction, which makes it an interesting channel to study. The process $pp \to tt\bar{t} + W^-$ has the larger cross-section as compared to other processes at different center-of-mass energies.

5. Four top-quark production

Four top quarks have two production modes: quark–antiquark annihilation and gluon–gluon fusion. The gluon–gluon fusion process is dominant at the LHC. The gluon–gluon fusion has a contribution of 90% and quark–antiquark annihilation one of 10%. The cross-section of four top-quark production is around five orders of magnitude smaller than the top-pair production and so it has yet to be observed [25,26].

Table 4 shows the cross-section for quark–antiquark annihilation ($q\bar{q} \to t\bar{t}t\bar{t}$) and gluon–gluon fusion ($gg \to t\bar{t}t\bar{t}$) at different center-of-mass energies for four top-quark production. In

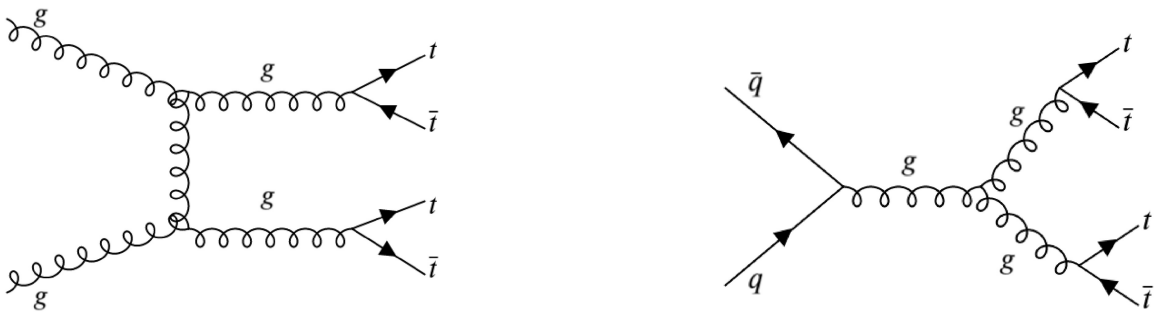

Fig. 7. Feynman diagrams for four top-quark production in the SM at the LHC corresponding to quark–antiquark annihilation and gluon–gluon fusion processes.

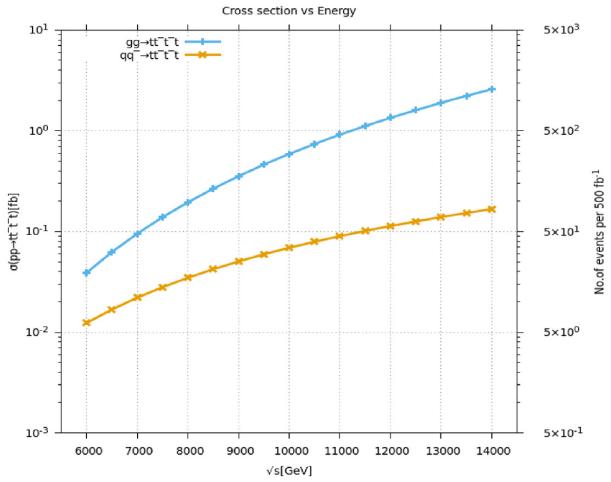

Fig. 8. Cross-section for four-top production in the SM for different LHC center-of-mass energies.

Fig. 7 and Fig. 8 the Feynman diagrams and their cross section plot is shown. Table 5 shows cross-section detail of signal and background processes at Next to Leading Order (NLO). In Fig. 9, the production cross-section of all four most likely produced processes and corresponding number of produced events at integrated luminosity of 500 fb^{-1} are shown as a function of center of mass energy in the femto barn.

6. Signal and background processes

In this study, various scattering mechanisms are used as signals. The $tt\bar{t}W$, $tt\bar{t}\bar{b}$, and $tt\bar{t}d$ are scattering processes. All of these scattering mechanisms are generated by proton–proton collisions at $\sqrt{s}$= 14 TeV. In all of the triple-top signal processes, hadronic decay of the W-boson is taken into account. In the $tt\bar{t}W$, $tt\bar{t}\bar{b}$, and $tt\bar{t}d$scattering processes, the top quark (t) decays into a W-boson and bottom quark (b). W decays to produce light jets (u, d, c, s). As a result, there are eleven jets in the final state of the scattering process $tt\bar{t}W$, consisting of eight light jets and three b-jets: $pp \rightarrow tt\bar{t}W \rightarrow 4W^{\pm} + 3bjets \rightarrow 8jets + 3bjets$. There are ten jets in the final state of the scattering process $tt\bar{t}\bar{b}$, which includes six light jets and four b-quark jets: $pp \rightarrow tt\bar{t}\bar{b} \rightarrow 3W^{\pm} + 4bjets \rightarrow 6jets + 4bjets$. Similarly, the $tt\bar{t}d$ scattering process produces ten jets, seven of which are light jets and three of which are b-jets: $pp \rightarrow tt\bar{t}d \rightarrow 3W^{\pm} + 3bjets \rightarrow 7jets + 3bjets$.

Table 5. Cross-sections of three signals and background processes are shown at three different energies using the Next-to-Next Leading Order parton density function.

$\sqrt{s}$ [TeV] [TeV]	$tt\bar{t}W$ fb	$t\bar{t}tb$ fb	$t\bar{t}td$ fb	$t\bar{t}h$ fb	$t\bar{t}Z$ fb	$t\bar{t}W$ fb	tWZ fb	WWZ fb	tZj fb
14	1.5	0.1	0.2	483	703	402	141	90	816
27	12.7	0.45	1.2	838	3329	1176	691	263	3142
100	352	3.5	13	11 490	44 800	6976	8970	1463	26 380

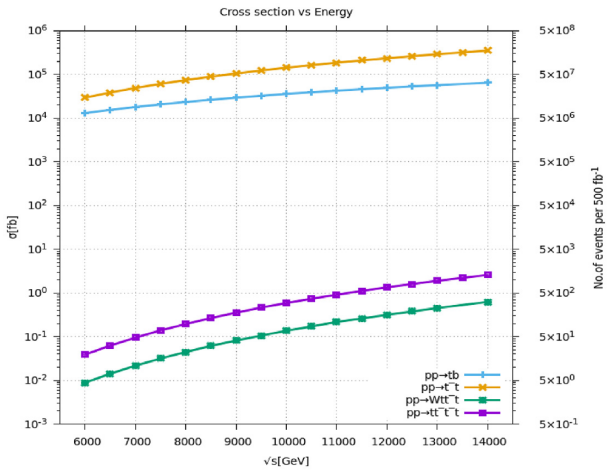

Fig. 9. Cross-section for single, pair, triple, and four top production in the SM for different LHC center-of-mass energies.

The following background processes of the SM with similar final state topologies are produced while analyzing these signal processes. In $t\bar{t}Z$, $t\bar{t}W^{\pm}$, and $W^{+}W^{-}Z$, a top quark decays into a W-boson and b-jet. When Z and W decay, they produce a pair of light jets. In $pp \to t\bar{t}Z \to 6$ jets $+ 2$ b-jets, $t\bar{t}W \to 6$ jets $+ 2$ b-jets, and in $W^{+}W^{-}Z \to 6$ jets.

7. Event selection and collider analysis

A complete analysis of the three processes whose cross-sections are presented in sect. 4 is studied. Three signal processes are explored where three top quarks are produced along with additional particles in each process and fully hadronic decay modes are selected. The parton density function is provided by LHAPDF 5.9.1 [27] with CTEQ version 6.6. The background processes $W^{+}W^{-}Z$, $t\bar{t}W^{\pm}$, and $t\bar{t}Z$ are generated with calchep [28] with a kinematic preselection cut applied on jets as $E_T^{jets} > 15$ GeV and $|\eta| < 3.0$ [29]. All the signal processes are also produced with Calchep. The output of both these packages is in Les Houches Event (LHE) format and used by PYTHIA8 for parton showering, gluon radiation, fragmentation, and hadronization. PYTHIA calculates their relative efficiency as well. The HepMC v2.06.09 interface with PYTHIA is then used to record events. FastJet v3.3.4 is then coupled with PYTHIA for jet definition and reconstruction. The jet cone size is fixed at $\Delta R = 0.4$, where $\Delta R = \sqrt{(\Delta\eta)^2 + (\Delta\phi)^2}$ is jet cone radius, ϕ is azimuthal angle, and $\eta = -ln\tan\theta/2$ is pseudorapidity. The output is then analysed with ROOT v6.14.06. In this study, various scattering mechanisms are used as signals. The $tt\bar{t}W$, $tt\bar{t}\bar{b}$, and $tt\bar{t}d$ are scattering processes. All of these scattering mechanisms are generated by p–p collisions at $\sqrt{s}$= 14 TeV at the HL-LHC and $\sqrt{s}$= 27 TeV center-of-mass energy at the

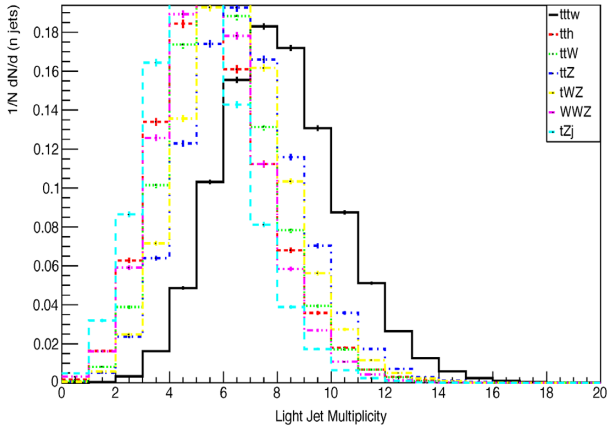

Fig. 10. The jet multiplicity distributions of both signal and background events are shown at $\sqrt{s}$= 14 TeV.

High-Energy LHC (HE-LHC). In all of the triple-top signal processes, a hadronic decay of the W-boson is taken into account.

Various selection cuts are used to reduce background while keeping the signal. The chi-square method is used to reconstruct the physics objects in which we are interested. Several kinematic variables are plotted during the entire analysis to examine the distributions of W-bosons, top quarks, etc.

Jets are reconstructed using the Anti$-k_t$ technique with R and ΔR set to 0.4 in this investigation.

Some of the jets in this mechanism extend beyond the cone size due to a variety of causes such as detector impairment, magnetic field influence, and material influence. All of these jets are sorted by p_T and the following kinematic cut on jets is applied.

$$P_T^{l\text{jets}} \geq 15\,\text{GeV and } \mid \eta \mid \leq 2.5$$

The selected jets are then tagged as either a b-jet or a light jet. In order to to this, we do ΔR matching of jets with the parton level b- and c-quarks. Charm quarks are used to increase efficiency since their masses are closer to those of bottom quarks. The jets which are within $\Delta R < 0.2$ are identified as b-jets and all the other jets which are farther away from b-quarks are identified as light jets. Once the tagging is done, we apply a multiplicity cut on jets. In the analysis of $tt\bar{t}W$, there are eight light jets and three b-jets so we only keep the events where we have

$$N_{l\text{jets}} \geq 8, N_{b\text{jets}} \geq 3$$

Similarly, for $tt\bar{t}\bar{b}$, there are six light jets and four b-jets so the event selection cut becomes

$$N_{l\text{jets}} \geq 6, N_{b\text{jets}} \geq 4$$

and for process $tt\bar{t}d$

$$N_{l\text{jets}} \geq 7, N_{b\text{jets}} \geq 3$$

In Fig. 10 the light jet multiplicity of signal processes with their backgrounds is given. It can be seen that almost 20 percent of jets are passed through the jets kinematic cut. Also it can be seen that the jet multiplicity of the scattering processes is almost the same. It can be seen from Fig. 11 that there are prominent signals of b-jets . Distribution of pseudorapidity and transverse momentum of selected jets are also given in Fig. 12 and Fig. 13, respectively.

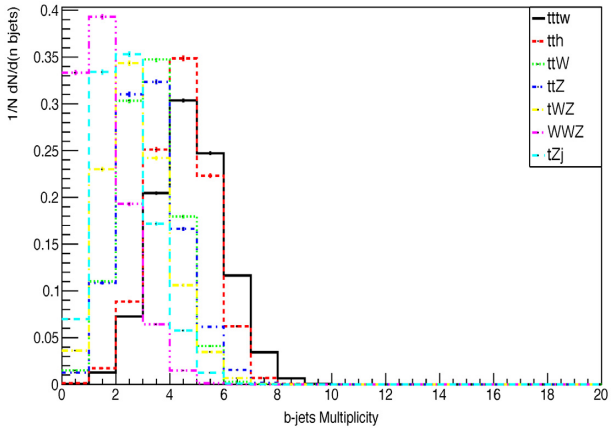

Fig. 11. The b-jets multiplicity distributions in both signal and background events.

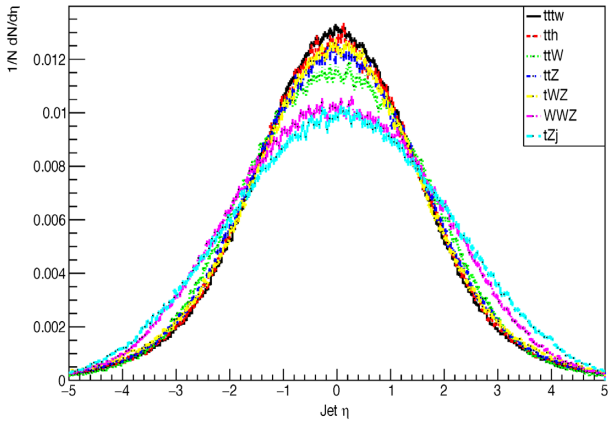

Fig. 12. Pseudorapidity distributions of signal and background selected jets at $\sqrt{s}$= 14 TeV.

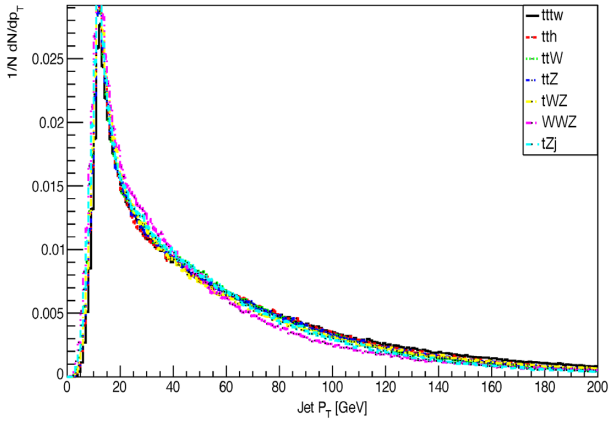

Fig. 13. Transverse momentum distributions of selected jets at $\sqrt{s}$= 14 TeV.

In the case of the $tt\bar{t}\bar{b}$ scattering process four b-jets efficiency is in the range of 50 percent. But in the cases of $tt\bar{t}d$ and $tt\bar{t}W$ it increases up to 75 percent–80 percent. The presence of SM backgrounds as compared to signal is low. Figure 11 shows the distributions of b-jet multiplicities for various signals and backgrounds.

8. Reconstruction of invariant masses

In particle physics, the invariant mass is defined as its mass in the rest frame and is given as

$$m_0 c^2 = \left(\frac{E}{c}\right)^2 - \mid p \mid^2 \tag{1}$$

Set $c = 1$ for convenience,

$$m_0 = (E)^2 - \mid p \mid^2 \tag{2}$$

After selecting desired events from randomly produced events, the reconstruction of invariant masses from the product of decays is the next step. First, the invariant mass of the W-boson is reconstructed. For this, all events having at least eight jets for the $tt\bar{t}W$ signal, six jets for the $tt\bar{t}\bar{b}$ signal, and seven jets for the $tt\bar{t}d$ signal are chosen, and the invariant mass is reconstructed using all possible light jet pairs using the following formula:

$$\mathbf{m_{j_1 j_2}} = \sqrt{(\mathbf{E_{j_1}} + \mathbf{E_{j_2}})^2 - (p_{\mathbf{x_{i_1}}} + p_{\mathbf{x_{i_2}}})^2 - (p_{\mathbf{y_{i_1}}} + p_{\mathbf{y_{i_2}}})^2 - (p_{\mathbf{z_{i_1}}} + p_{\mathbf{z_{i_2}}})^2} \tag{3}$$

9. Chi-square method

The chi-square method is then used to reconstruct the physics object of interest with the correct invariant mass. For reconstruction of the W-boson, we check the invariant mass of di-jet objects and choose the six jets that give the minimal value of chi-square defined as,

$$\chi^2_W = \sum_{i=1}^{3} \left(\frac{m_{i,jj} - m_W}{\sigma_{m,jj}}\right)^2 \tag{4}$$

where $m_{i,jj}$ is the di-jet mass, m_W is the mass of the W-boson, and $\sigma_{m,jj}$ is the width of the di-jet mass distribution obtained from the parton-matched jets. The events are only selected if the $\chi^2_{W,min} < 10$. Once the W's are reconstructed, we again apply the same method to reconstruct top quark candidates using the selected b-jets and the reconstructed W's.

$$\chi^2_t = \sum_{i=1}^{3} \left(\frac{m_{i,jjb} - m_t}{\sigma_{m,jjb}}\right)^2 \tag{5}$$

where the light jets are the ones chosen to make W-bosons, $m_{i,jjb}$ is a tri-jet mass, m_t is the mass of the top quark, and $\sigma_{m,jjb}$ is the width of the tri-jet distribution. Once again, the event is only selected if $\chi^2_{t,min} < 10$.

10. Event selection efficiencies

In this study, 80 000 events are generated and combined for signal processing in order to improve simulation results on selected kinematical cuts. Then signal efficiency corresponding to each selection cut is computed and then, at the end, total efficiency is calculated. Total efficiency corresponds to nine jet final states obtained at the end of the simulation, which consists of six light jets coming from three W-boson decay and b-jets resulting from top-quark decay. All these efficiencies are calculated at center-of-mass energy 14 TeV. All these efficiencies are mentioned in Tables 6, 7, and 8. The QCD k-factor values of $t\bar{t}Z$, $t\bar{t}W$, and $t\bar{t}H$ are written in Table 6, which are calculated by taking the ratio of σ_{NLO} over σ_{LO} of the given process reported in [30], [31], and [32], respectively. It can be seen that the efficiency of light jets for various kinematical cuts ranges from 15 percent to 26 percent for signals. In addition, the efficiency of b-jet production ranges from 50 percent to 80 percent for signals. The total efficiency of

Table 6. Signal $tt\bar{t}W$ and SM background process efficiencies at various kinematics and selection cuts.

Process	$tt\bar{t}W$	$t\bar{t}Z$	$t\bar{t}W$	$t\bar{t}H$	tWZ	tZj	WWZ
$N_{ljets} \leq 8$	0.49	0.25	0.14	0.13	0.20	0.06	0.10
$N_{bjets} \leq 3$	0.86	0.38	0.34	0.76	0.20	0.08	0.017
$\chi^2_{W,min} < 10$	0.87	0.87	0.85	0.86	0.85	0.80	0.78
$\chi^2_{t,min} < 10$	0.89	0.85	0.89	0.91	0.78	0.81	0.62
Total efficiency	0.32	0.07	0.037	0.08	0.02	0.003	0.001
K factor	–	1.27	1.24	1.21	–	–	–
Total efficiency	0.32	0.09	0.045	0.097	0.02	0.003	0.001

Table 7. Signal $tt\bar{t}\bar{b}$ and SM background process efficiencies at various kinematics and selection cuts.

Process	$tt\bar{t}\bar{b}$	$t\bar{t}Z$	$t\bar{t}W$	$t\bar{t}H$	tWZ	tZj	WWZ
$N_{ljets} \leq 6$	0.61	0.62	0.48	0.41	0.58	0.30	0.40
$N_{bjets} \leq 4$	0.60	0.14	0.12	0.48	0.066	0.014	0.003
$\chi^2_{W,min} < 10$	0.87	0.86	0.84	0.86	0.83	0.78	0.74
$\chi^2_{t,min} < 10$	0.84	0.83	0.87	0.88	0.79	0.75	0.75
Total efficiency	0.27	0.063	0.041	0.15	0.025	0.003	0.001
K factor	–	1.27	1.24	1.21	–	–	–
Total efficiency	0.27	0.08	0.050	0.18	0.025	0.003	0.001

Table 8. Signal $tt\bar{t}d$ and SM background process efficiencies at various kinematics and selection cuts.

Process	$tt\bar{t}d$	$t\bar{t}Z$	$t\bar{t}W$	$t\bar{t}H$	tWZ	tZj	WWZ
$N_{ljets} \leq 7$	0.47	0.42	0.28	0.26	0.38	0.15	0.22
$N_{bjets} \leq 3$	0.81	0.40	0.37	0.78	0.22	0.088	0.02
$\chi^2_{W,min} < 10$	0.96	0.97	0.97	0.98	0.96	0.95	0.93
$\chi^2_{t,min} < 10$	0.706	0.69	0.76	0.79	0.60	0.56	0.55
Total efficiency	0.26	0.12	0.081	0.16	0.049	0.007	0.002
K factor	–	1.27	1.24	1.21	–	–	–
Total efficiency	0.26	0.15	0.1	0.19	0.049	0.007	0.002

top-mass reconstruction and nine jet final states for the specified signal situation is very low, ranging from 6 percent to 8 percent.

11. Signal significance

To test the observability of the triple-top mass at various kinematical cuts, signal significance is calculated for each triple-top mass distribution shown in the figures from 6.31 to 6.39 by incorporating the total number of signal and background candidate masses within the selected mass limit. Signal significance is calculated using integrated luminosity 3000 fb^{-1}. The computed results, which include signal S and background B of candidate masses, signal to background ratio S/B, and signal significance $S/\sqrt{B}$ at $\sqrt{s} = 14$ TeV and 27 TeV, are shown in Tables 9 and 10. Figure 14 shows that at 14 TeV, the background is more dominant than the signal. As a result, the signal is not detectable because the cross-section of the triple top is very low even at 14 TeV. While in Fig. 15 ploted at 27 TeV, the signal is observable over background.

Table 9. Signal to background ratio and signal significance values obtained for three different triple-top production processes with maximum integrated luminosity 5000 fb^{-1} at the HL-LHC ($\sqrt{s}$= 14 TeV).

Signal process	Mass window		Total efficiency	No. of events	S/B	Optimized
	Lower limit	Upper limit				$S/\sqrt{B}$
$t\bar{t}tW^+$ Signal	186	294	0.11	282	0.003	1.045
Total background	186	294		73 143		
$t\bar{t}tb$ Signal	280	287	0.0002	0.03	0.0001	0.002
Total background	280	287		325		
$t\bar{t}td$ Signal	280	287	0.0003	0.12	0.0003	0.006
Total background	280	287		403		

Table 10. Signal to background ratio and signal significance values obtained for three different triple-top production processes with maximum integrated luminosity 5000 fb^{-1} at the HE-LHC ($\sqrt{s}$= 27 TeV).

Signal process	Mass window		Total efficiency	No. of events	S/B	Optimized
	Lower limit	Upper limit				$S/\sqrt{B}$
$t\bar{t}tW^+$ Signal	280	287	0.0001	2.27	0.003	0.1
Total background	280	287		628		
$t\bar{t}tb$ Signal	280	287	0.0003	0.22	0.0002	0.006
Total background	280	287		1441		
$t\bar{t}td$ Signal	248	296	0.0002	0.03	0.001	0.007
Total background	248	296		24		

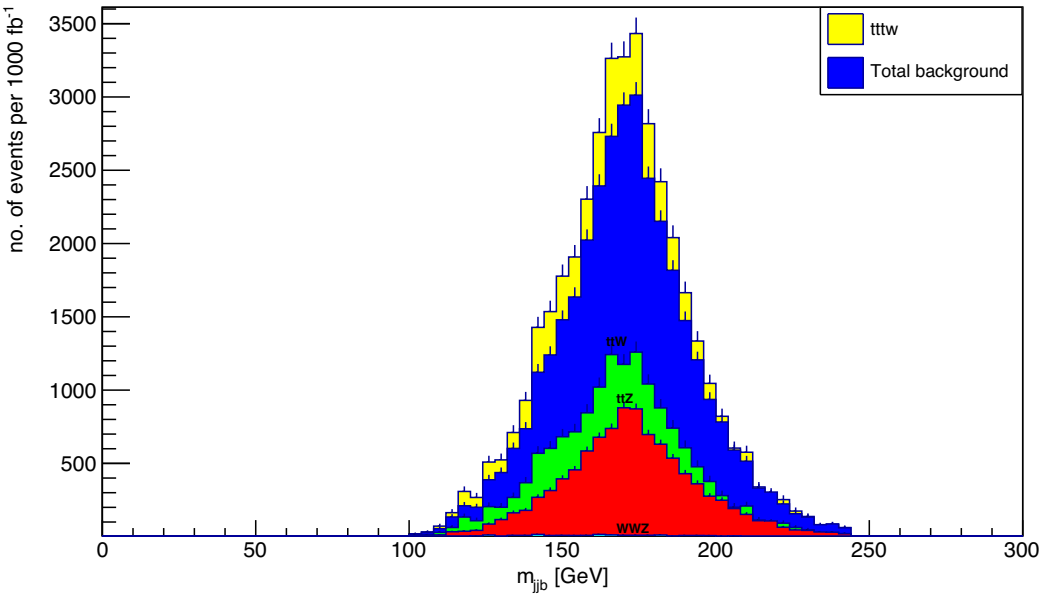

Fig. 14. Candidate mass distribution of triple top at integrated luminosity 3[ab^{-1}] at $\sqrt{s} = 14$ TeV.

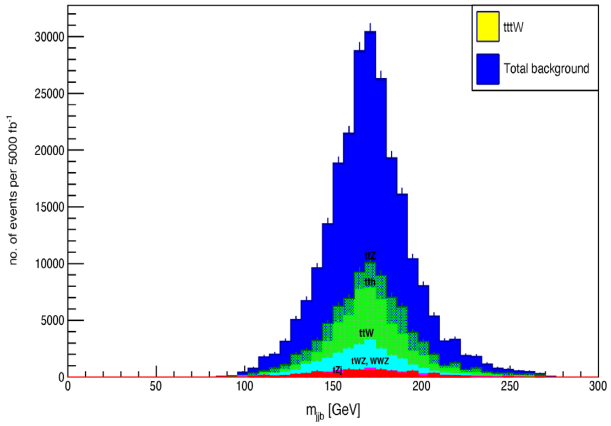

Fig. 15. The signal and background samples are normalized to the real number of events obtained at 5000 fb^{-1}.

Because the production process $tt\bar{t}W$ has the largest cross-section for both $\sqrt{s} = 14$ TeV and $\sqrt{s} = 27$ TeV, its S/B ratio is 1. As a result, the triple top has observability chances with the production process $tt\bar{t}W$ for both the LHC and HE-LHC. The other two processes have very low cross-sections and signal significance.

12. Conclusion

In the scope of the SM, various channels of triple-top quark generation are considered. This analysis of triple-top production shows that it has a very low cross-section when compared to other top-quark production modes. The mass of the triple top is reconstructed using hadronic decay of the top quark at $\sqrt{s}$= 14 TeV. The calculation of the signal to background ratio and signal significance clearly shows that at $\sqrt{s}$= 14 TeV and $\sqrt{s}$= 27 TeV, not all signal scenarios are observable. Only $tt\bar{t}W$ has a signal to background ratio of one. At the LHC the backgrounds are dominant and the signal is not visible because of the very low cross-section. Due to the low SM rate, it is conceivable to explore for contributions that are beyond the scope of the SM (BSM), which may improve the cross-section. Specific computations, however, are required to study actual BSM aspects.

Funding

Open Access funding: SCOAP[3].

References

[1] D. Wicke, Single and double top quark production at the Tevatron. (2010) In arXiv preprint[arXiv:1006.1275] [Search inSPIRE].
[2] Y. P. Gouz and S. R. Slabospitsky, Phys. Lett. B, (1999).
[3] K. Masaya, M. Tanmoy, and W.-S. Hou, Phys. Lett. **B776**, 379 (2018).
[4] S. Cho, P. Ko, J. Lee, Y. Omura, and C. Yu, Phys. Rev. D **101**, 055015 (2020).
[5] B. Gomez, P. Mooney, J. P. Negret, J. M. R. Roldan, D. Fein, G. E. Forden, E. James, K. Johns, L. Markosky, and A. Milder, others, Phys. Rev. Lett., (1995).
[6] D. Chakraborty, J. Konigsberg, and D. Rainwater, Annual Rev. of Nuclear and Particle Sci. (2003).
[7] P. Bärnreuther, Top quark pair production at the LHC, (2012).
[8] S. Abachi, B. Abbott, M. Abolins, B. S. Acharya, I. Adam, D. L. Adams, M. Adams, S. Ahn, H. Aihara, and J. Alitti, others, Phys. Rev. Lett. (1995).

[9] M. Beneke, I. Efthymiopoulos, M. L. Mangano, J. Womersley, A. Ahmadov, G. Azuelos, U. Baur, A. Belyaev, E. L. Berger, W. Bernreuther, E. E. Boos, M. Bosman, A. Brandenburg, R. Brock, M. Buice, N. Cartiglia, F. Cerutti, A. Cheplakov, L. Chikovani, M. Cobal-Grassmann, G. Corcella, F. del Aguila, T. Djobava, J. Dodd, V. Drollinger, A. Dubak, S. Frixione, D. Froidevaux, B. Gonzalez Pineiro, Y. P. Gouz, D. Green, P. Grenier, S. Heinemeyer, W. Hollik, V. Ilyin, C. Kao, A. Kharchilava, R. Kinnunen, V. V. Kukhtin, S. Kunori, L. La Rotonda, A. Lagatta, M. Lefebvre, K. Maeshima, G. Mahlon, S. Mc Grath, G. Medin, R. Mehdiyev, B. Mele, Z. Metreveli, D. O'Neil, L. H. Orr, D. Pallin, S. Parke, J. Parsons, D. Popovic, L. Reina, E. Richter-Was, T. G. Rizzo, D. Salihagic, M. Sapinski, M. H. Seymour, V. Simak, L. Simic, G. Skoro, S. R. Slabospitsky, J. Smolik, L. Sonnenschein, T. Stelzer, N. Stepanov, Z. Sullivan, T. Tait, I. Vichou, R. Vidal, D. Wackeroth, G. Weiglein, S. Willenbrock, and W. Wu, Top quark physics. *arXiv preprint hep-ph/0003033*, (2000) [Search INSPIRE].
[10] A. Giammanco, Rev. in Phys. (2016).
[11] N. Bruscino and ATLAS Collaboration, others, Physica Scripta (2020).
[12] F. Déliot and P. Van Mulders, Comptes Rendus. Physique, (2020).
[13] C. Young, Top Quark Properties from ATLAS, (2020).
[14] J. R. Incandela, A. Quadt, W. Wagner, and D. Wicke, Progress in Particle and Nuclear Physics (2009).
[15] V. Barger, W.-Y. Keung, and B. Yencho, Phys. Lett. B (2010).
[16] Q.-H. Cao, S.-L. Chen, Y. Liu, and X.-P. Wang, Phys. Rev. D, (2019).
[17] T. M. P. Tait and C.-P. Yuan, Phys. Rev. D (2000).
[18] ATLAS collaboration, others, Journal of High Energy Phys. (2020).
[19] W. Bernreuther, Journal of Physics G: Nuclear and Particle Physics (2008).
[20] V. M. Abazov, B. Abbott, M. Abolins, B. S. Acharya, M. Adams, T. Adams, E. Aguilo, M. Ahsan, G. D. Alexeev, and G. Alkhazov, others, Phys. Rev. Lett. (2009).
[21] K. Kröninger, A. B. Meyer, and P. Uwer, The Large Hadron Collider, 259 Springer, (2015).
[22] T. Han, Perspectives on LHC Physics (2008).
[23] E. Boos and L. Dudko, (2021) arXiv preprint[arXiv:2107.07629] [Search inSPIRE].
[24] H. Khanpour, Nuclear Physics B, (2020).
[25] CMS collaboration, others, (2017) arXiv preprint[arXiv:1702.06164] [Search inSPIRE].
[26] A. M. Sirunyan, A. Tumasyan, W. Adam, E. Asilar, T. Bergauer, J. Brandstetter, E. Brondolin, M. Dragicevic, J. Erö, and M. Flechl, Eur. Phys. J. **C80**, 75 (2020).
[27] M. R. Whalley, D. Bourilkov, and R. C. Group, arXiv preprint hep-ph/0508110, (2005) [Search INSPIRE].
[28] A. Belyaev, N. D. Christensen, and A. Pukhov, Computer Physics Communications (2013).
[29] T. Sjöstrand, S. Mrenna, and P. Skands, Computer Physics Communications (2008).
[30] G. Bevilacqua, H. B. Hartanto, M. Kraus, J. Nasufi, and M. Worek, J. High Energy Phys. **08**, 060 (2022).
[31] J. M. Campbell and R. Keith Ellis, J. High Energy Phys. **07**, 052 (2012).
[32] D. Stremmer and M. Worek, J. High Energy Phys. **02**, 196 (2022).